

Modeling, Simulation and Control of a Tubular Fixed-bed Dimethyl Ether Reactor

E. Yasari,^a M. Shahrokhi,^{a,*} and H. Abedini^b

^aDepartment of Chemical & Petroleum Engineering, Sharif University of Technology, P. O. Box 11365-9465, Tehran, Iran

^bDepartment of Polymerization Engineering, Iranian Polymer and Petrochemical Institute, Tehran, Iran

Original scientific paper

Received: March 15, 2010

Accepted: September 13, 2010

This paper considers the modeling and control of a tubular fixed bed reactor with recycle stream for dimethyl ether (DME) production. For simulation purposes, a pseudo homogeneous model has been developed. By reactor simulation under steady state condition, effects of parameters such as feed rate, pressure and shell temperature are investigated. Using the steady state model, an optimizer that maximizes the reactor yield has been developed. For cooling the reactor, a steam drum that uses heat of reactions to produce steam was coupled with the reactor. Through dynamic simulation, system open loop response was obtained and two control loops were considered for controlling the reactor temperature and steam drum level. An optimizer that takes into account the feed variations was incorporated into the control system to maximize the DME production rate.

Key words:

Dimethyl ether, dynamic modelling, optimization, fixed bed reactor

Introduction

Dimethyl ether (DME) has been known as an ultra clean fuel that can be used in diesel engines, power generation and for other purposes.^{1,2} DME has many excellent characteristics and is identified as a potential diesel fuel. It contains 34.78 % oxygen and can be burned without soot emission, while for traditional diesel fuels one cannot expect simultaneous NO_x and soot emission control. It has a boiling point of -25 °C, which is 20 °C higher than liquefied petroleum gas (LPG) and can be liquidized at 0.54 MPa (20 °C). Therefore, no serious problem exists for the storage, transportation and usage of DME.³

Production of DME in one step in a slurry reactor was proposed by Air Product and Chemicals, Inc.⁴ This kind of reactor can provide efficient heat management. This is demonstrated by the experimental results reported by Du *et al.*⁵ and Guo *et al.*⁶

In the Haldor Topsoe process, the fixed-bed reactor was used. The reaction was carried out in a series of adiabatically operating reactors with inter-stage coolers. Adiabatic reactors are preferred because of their simpler design and easy operation, but for highly exothermic reactions the temperature rise is unacceptable.

Considerable works have been done on the simulation of packed-bed and adiabatic reactors and few of them are cited in what follows. Lee presented a general solution for solving nonlinear partial differential equations describing dynamics of packed-bed

reactors for isothermal and adiabatic operations using Newton-Raphson method.⁷ Cresswell and Pater-son developed a one-dimensional (1D) model for a system of gas-solid reaction and obtained an analytical solution.⁸ Balakotaiah *et al.* investigated the temperature and concentration gradients in axial and radial directions for an adiabatic packed-bed reactor.⁹ Baghmisheh and Shahrokhi have simulated dynamic behavior of a fixed-bed reactor for methanol production and proposed an optimizer for maximizing the production rate.¹⁰ Cho *et al.* have analyzed one-step DME synthesis from syngas in a shell and tube type fixed bed reactor with consideration of heat and mass transfer between catalyst pellets and reactants in the gas phase.¹¹ Yoon *et al.* have conducted simulations using a one-dimensional steady-state model of a heterogeneous catalyst bed. They have simulated the reactor under steady-state conditions and compared the simulation results with the data obtained from a pilot-scale reactor. Moreover, they considered the effectiveness factor for the catalyst pellets and obtained temperature and concentration profiles along the reactor.¹²

Since the reactions involved in DME production are highly exothermic, a reactor with efficient heat removal is required. In this work, a catalytic shell and tube fixed bed reactor, like the Lurgi methanol reactor, has been proposed for DME production. For cooling the reactor, a steam drum using heat of reactions to produce steam has been coupled with the reactor. To maximize the DME production rate, an optimizer has been coupled with the control system. Effectiveness of the proposed scheme has been demonstrated through computer simulation.

*Corresponding author. Tel: +982166165419; Fax: +982166022853
E-mail address: Shahrokhi@sharif.edu

Process description

Reactions involved in the DME production are highly exothermic and therefore reactor temperature control is a challenging problem. In this work, the catalytic shell and tube fixed-bed reactor, used by Lurgi for the methanol process, has been proposed for DME production. This kind of reactor can provide efficient heat removal from the reactor and the temperature can be controlled effectively.

The schematic diagram of the process is shown in Fig. 1. A mixture of fresh feed and recycled stream enters the reactor after being heated in a heat exchanger. The outlet stream of the reactor is cooled and enters a separator where liquid is separated as product and the non-condensed DME and unreacted gas are recycled into the reactor. A fraction of recycled gas is purged to prevent accumulation of inert components. For cooling the reactor, a steam drum was coupled with the reactor. The heat of reaction was removed by generating the steam that leaves the steam drum through a control valve.

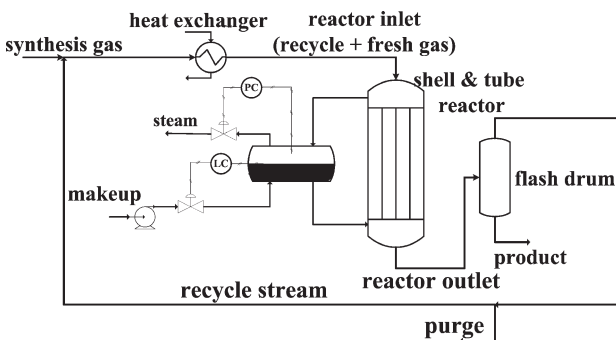


Fig. 1 – Schematic diagram of DME synthesis loop

Reaction kinetics

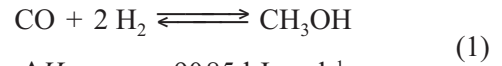
The kinetics represented by Nie *et al.* were selected for DME production based on the Langmuir-Hinshelwood and Hougen-Watson mechanism.¹³ This model has been validated experimentally.¹³

The eight components used in this kinetic model are:

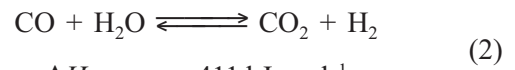
H₂, CO, CO₂, H₂O, methanol, DME, N₂, and CH₄ (as inert components).

The main reactants are H₂ and CO and the presence of inert components that absorb part of the heat of reaction, facilitate control of the reactor.

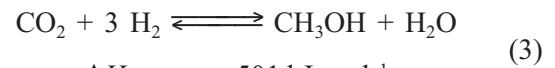
In three synthesis approaches of dimethyl ether, namely CO hydrogenation, CO₂ hydrogenation, and parallel hydrogenation of CO and CO₂, the following four reactions are involved:¹⁴



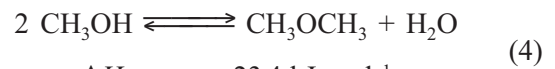
$$\Delta H_{25^\circ\text{C}} = -90.85 \text{ kJ mol}^{-1}$$



$$\Delta H_{25^\circ\text{C}} = -41.1 \text{ kJ mol}^{-1}$$



$$\Delta H_{25^\circ\text{C}} = -50.1 \text{ kJ mol}^{-1}$$



$$\Delta H_{25^\circ\text{C}} = -23.4 \text{ kJ mol}^{-1}$$

The above reactions are not independent and each reaction can be obtained from a combination of the remaining three reactions.¹⁴ In this work, reactions 1, 3 and 4 were considered for simulating the reactor behavior.

The reaction rates proposed by Nie *et al.* were used, as given below:¹³

$$r_{\text{CO}} = \frac{k_1 f_{\text{CO}} f_{\text{H}_2}^2 (1 - \beta_1)}{(1 + K_{\text{CO}} f_{\text{CO}} + K_{\text{CO}_2} f_{\text{CO}_2} + K_{\text{H}_2} f_{\text{H}_2})^3} \quad (5)$$

$$r_{\text{CO}_2} = \frac{k_2 f_{\text{CO}_2} f_{\text{H}_2}^3 (1 - \beta_2)}{(1 + K_{\text{CO}} f_{\text{CO}} + K_{\text{CO}_2} f_{\text{CO}_2} + K_{\text{H}_2} f_{\text{H}_2})^4} \quad (6)$$

$$r_{\text{DME}} = \frac{k_3 f_{\text{CH}_3\text{OH}} (1 - \beta_3)}{(1 + \sqrt{K_{\text{CH}_3\text{OH}} f_{\text{CH}_3\text{OH}}})^2} \quad (7)$$

where

$$\beta_1 = \frac{f_{\text{CH}_3\text{OH}}}{K_{f_1} f_{\text{CO}} f_{\text{H}_2}^2}, \quad \beta_2 = \frac{f_{\text{CH}_3\text{OH}} f_{\text{H}_2\text{O}}}{K_{f_2} f_{\text{CO}_2} f_{\text{H}_2}^3},$$

$$\beta_3 = \frac{f_{\text{DME}} f_{\text{H}_2\text{O}}}{K_{f_3} f_{\text{CH}_3\text{OH}}^2}$$

The kinetic parameters are given in Table 1.

Table 1 – Kinetic and equilibrium constants

Parameters	$A_i \exp(E_i/(RT))$	
	A_i	$E_i/\text{J mol}^{-1}$
$k_1/\text{mol s}^{-1} \text{ kg}^{-1} \text{ bar}^{-3}$	7.38e3	-54307
$k_2/\text{mol s}^{-1} \text{ kg}^{-1} \text{ bar}^{-4}$	5.059e3	-67515
$k_3/\text{mol s}^{-1} \text{ kg}^{-1} \text{ bar}^{-1}$	1.063e3	-43473
$K_{\text{CO}}/\text{bar}^{-1}$	3.934e-6	37373
$K_{\text{CO}_2}/\text{bar}^{-1}$	1.858e-6	53795
$K_{\text{H}_2}/\text{bar}^{-1}$	0.6716	-6476
$K_{\text{CH}_3\text{OH}}/\text{bar}^{-1}$	3.48e-6	54689

Modeling and simulation

A one-dimensional (1D) pseudo homogeneous model was used to model the reactor. The assumptions are listed below.

1. Since $L/D > 100$, radial variations are not considered, where L is the reactor length and D is the reactor diameter.

2. The axial dispersions of mass and energy are neglected.

3. Internal and external diffusions are not taken into account.¹⁵

4. The effectiveness factor is assumed to be one.¹⁵

From the kinetic point of view, conversion rates of syngas and CO_2 into DME were relatively slow and consequently diffusion resistance was neglected.¹⁵

Reactor mathematical model

One-dimensional and pseudo-homogeneous model was considered for simulating the tubular fixed-bed DME reactor. Mass and energy balances are given below.

Mass balance:¹⁸

$$\varepsilon C \frac{\partial}{\partial t} x_i = -\frac{\varepsilon c u_s}{L_r} \frac{\partial}{\partial z} x_i + \rho_s \left(\sum_{j=1}^{n_r} v_{ij} r_j - x_i \sum_{i=1}^{n_c} \sum_{j=1}^{n_r} v_{ij} r_j \right) \quad (8)$$

Energy balance:¹⁰

$$\hat{C}_{p,m} \frac{\partial T}{\partial t} = -\frac{u_s C_{p,g} \rho_g}{L_r} \frac{\partial T}{\partial z} + \left(\rho_b \left(\sum_{i=1}^{n_r} (-\Delta H)_i r_i \right) + \frac{4U_{\text{eff}}}{d_{\text{out}}} (T - T_C) \right) \quad (9)$$

where $\hat{C}_{p,m} = (\varepsilon \rho_g c_{p,g} + (1 - \varepsilon) \rho_s c_{p,s})$ and U_{eff} is the overall heat transfer coefficient, calculated by the correlation given in the literature.¹⁸

For the pressure drop, the Ergun equation has been used:

Gas pressure drop:

$$\frac{d}{dz} p = -10^{-5} L_r \left(1.75 + 150 \left(\frac{1 - \varepsilon}{d_p \rho_g u_s / \mu_g} \right) \right) \cdot \frac{u_s^2 \rho_g}{d_p} \frac{1 - \varepsilon}{\varepsilon^3} \quad (10)$$

Variable z in the above equations is the dimensionless length defined as $z = x/L_r$.

The initial and boundary conditions are given below.

Boundary conditions: $x_i|_{z=0} = x_{i,\text{inlet}}$,

$T|_{z=0} = T_{\text{inlet}}$, $p|_{z=0} = p_{\text{inlet}}$.

Initial conditions: $x_i|_{z,t=0} = x_i^{\text{ss}}$, $T|_{z,t=0} = T^{\text{ss}}$.

The composition of fresh feed is: $x_{\text{H}_2} = 68.47$, $x_{\text{CO}} = 23.10$, $x_{\text{CO}_2} = 6.96$, $x_{\text{H}_2\text{O}} = 0.18$, $x_{\text{N}_2} = 0.29$, $x_{\text{CH}_4} = 0.98$. System parameters are given in Table 2.

Table 2 – Reactor parameters

diameter of each pipe, d/mm	38
length of each pipe, L_r/m	9.144
number of pipes, N	2676
catalyst diameter, d_p/mm	5.4
catalyst density, $\rho_c/\text{kg m}^{-3}$	1982.5
porosity, ε	0.4

Steam drum modeling

The model proposed by Luyben¹⁶ and Ramirez¹⁷ was used for steam drum modeling. The following assumptions were made:

1. Pseudo-steady state condition considered for vapor phase in writing the energy balance.

2. Energy loss neglected.

The schematic diagram of the steam drum is shown in Fig. 2.

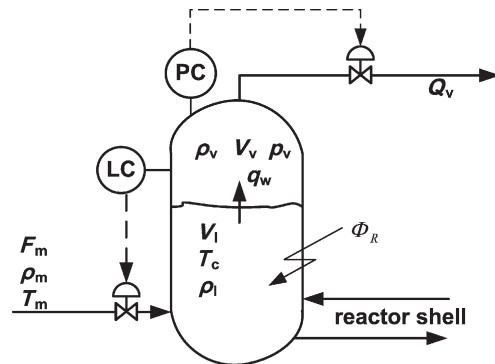


Fig. 2 – Steam drum schematic diagram

Mass balance for liquid phase:

$$\frac{d(\rho_l V_l)}{dt} = \rho_m Q_m - q_w \quad (11)$$

Mass balance for gas phase:

$$\frac{d(\rho_v V_v)}{dt} = q_w - \rho_v Q_v \quad (12)$$

Energy balance for liquid phase:

$$\frac{d(C_{p,1}\rho_1V_1T_C)}{dt} = \rho_m Q_m h_m - h_s q_w + \Phi_R \quad (13)$$

where

$$q_w = K_{MT}(p^{\text{sat}} - p_v) \quad (14)$$

$$p_v = \frac{z_s \rho_v RT_C}{MW_{\text{water}}} \quad (15)$$

$$Q_V = K_V \sqrt{p_v(p_v - p_0)} \quad (16)$$

Parameters K_{MT} and K_V are pseudo-mass transfer and control valve coefficients respectively.¹⁶

Numerical solution

First, the system under steady state conditions was simulated by Ode solver of MATLAB software in variable step size mode with respect to the axial direction. The obtained variable step sizes in axial direction were used for discretization of partial-differential equations (governing equations for unsteady condition) and converting them into ordinary differential equations (ODEs). The resulting set of these ODEs plus steam drum equations are solved by MATLAB Ode solver in variable step mode respect to time, simultaneously.

Two steady state simulations were performed, one using the ideal gas law and the other using the SRK equation for the gas phase. The results are given in Table 3. As can be seen, the error caused due to using ideal gas law is negligible and therefore the rest of the simulations are performed using the ideal gas law for the gas phase.

Table 3 – Simulation results of tubular reactor using ideal gas law and SRK equations

Results	SRK	Ideal gas	Relative error/%
conversion, $X_{CO}/\%$	82.898	82.793	0.126662
conversion $X_{H_2}/\%$	17.111	17.071	0.233768
DME product, $F_{DME}/\text{mol s}^{-1}$	133.9970	133.7878	0.156123
outlet temperature, $\vartheta_0/^\circ\text{C}$	247.78	247.77	0.00192

Effect of operating conditions on the reactor performance

It should be noted that in all simulation runs the mass flow rate of recycle stream was fixed (16.085 kg s^{-1}).

Effect of fresh feed flow rate

To investigate the effect of the fresh feed flow rate on the reactor performance, it was changed by $\pm 10\%$ and the results are shown in Fig. 3. As can be seen from Fig. 3a, increasing the feed flow rate, increases the maximum reactor temperature. This can be explained as follows. By increasing the fresh feed flow rate, reactants mole fractions are increased, leading to increase in reaction rates and heat generation, which in turn result in a higher reactor temperature. Fig. 3b shows variations of CO conversion along the reactor length. As can be seen, by increasing the feed flow rate, the CO conversion decreases. This can be justified as explained below. It is true that more CO is converted due to increase of the fresh feed flow rate as explained previously, but this does not necessarily imply that CO conversion increases. It should be noted that conversion is defined as:

$$X_i = \frac{n_{0i} - n_i}{n_{0i}}$$

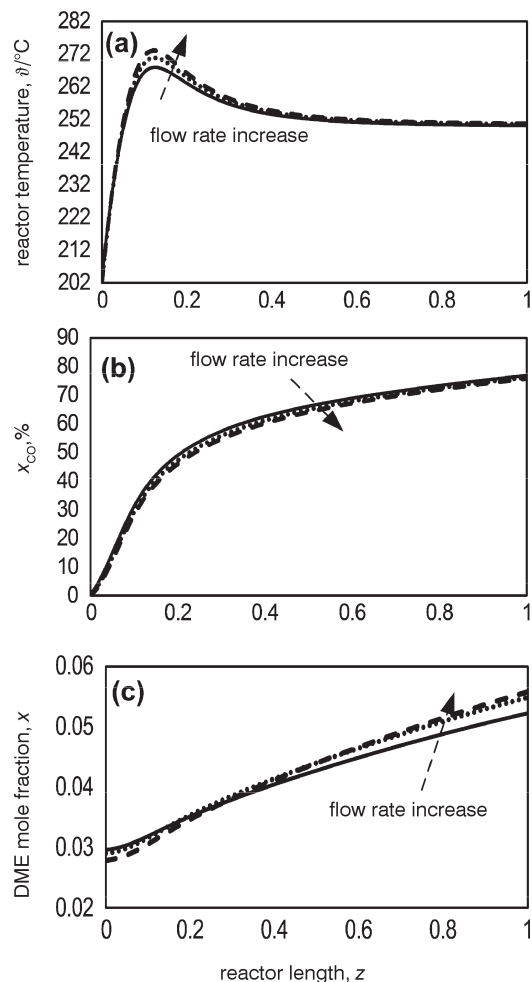


Fig. 3 – Effect of $\pm 10\%$ fresh feed flow rate changes on a) reactor temperature profile, b) CO conversion profile, c) DME mole fraction profile

Increasing the feed flow rate increases the numerator and denominator of the above equation. For the case under consideration, the increase in the denominator is more than the numerator, resulting in a decrease of CO conversion.

Variations of DME mole fraction are shown in Fig. 3c. As can be seen for both feed flow rate changes (decrease or increase), there is an intersection between the nominal curve and the one corresponding to the deviated feed flow rate. The mole fraction changes with respect to the base case are explained as follows. First, consider the feed flow rate reduction. As can be seen, a decrease in the fresh feed flow rate leads to a higher DME mole fraction in the reactor inlet. This can be explained as follows. From Fig. 3c it is observed that DME mole fraction at the reactor outlet is higher for the base case, indicating that the recycle stream of the base case has also a higher DME content. However, it should be noted that the recycle stream is mixed with the fresh feed and then enters the reactor. Decreasing the fresh feed flow rate decreases the reactor inlet feed flow, resulting in an increase of inlet DME mole fraction with respect to the base case despite a higher mole fraction of DME in the recycle stream of the base case.

Now, it is explained why the DME outlet mole fraction is higher for the base case with respect to lower feed flow rate case. Since the reactants content in the base case is higher, more CO is converted along the reactor, leading to a higher outlet DME mole fraction for the base case.

The same reasoning can be applied to justify the effect of increasing the fresh feed flow rate on DME mole fraction along the reactor.

Effect of pressure

Effects of pressure on DME production rate, CO conversion and reactor temperature are shown in Figs. 4a to 4c. As can be seen from the reaction kinetics, production of DME is accompanied by reduction of the total number of molecules. Therefore, increasing the pressure shifts the reactions towards the product side, which in turn results in a higher CO conversion and DME production. In addition, the maximum temperature in the reactor increases by increasing the inlet pressure which is harmful for DME catalyst.

Effect of shell temperature

The shell temperature strongly influences the DME yield and reactor thermal stability. If the DME production rate is plotted vs. shell tempera-

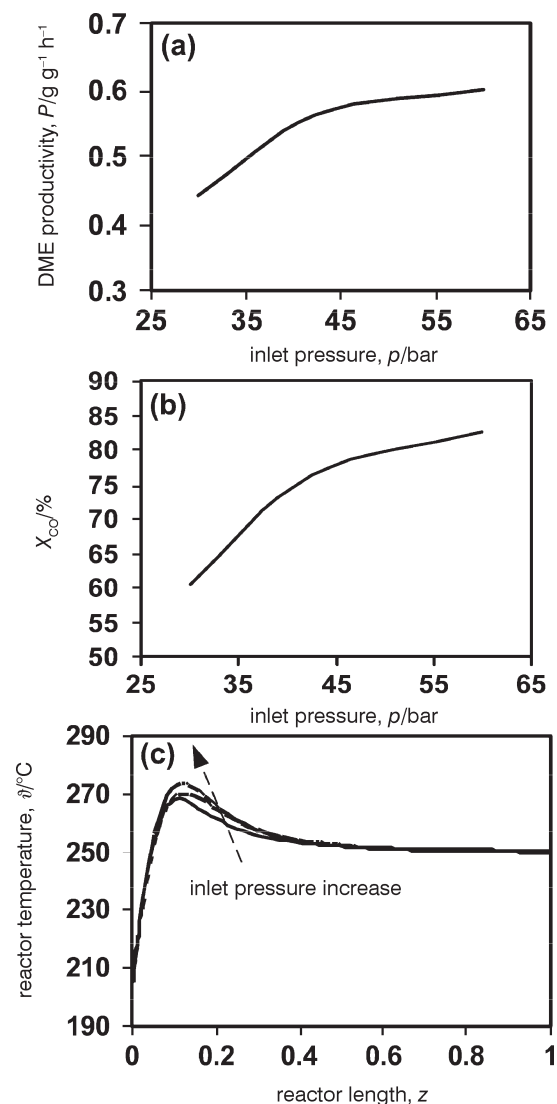


Fig. 4 – Effect of reactor pressure changes on a) DME productivity, b) CO conversion, c) reactor temperature profile

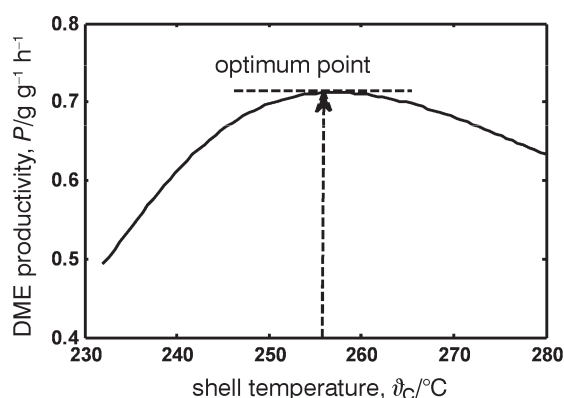


Fig. 5 – Effect of shell temperature on DME productivity at reactor outlet

ture, Fig. 5 is obtained. As can be seen, there is an optimum temperature that maximizes the DME productivity for a given feed composition. However,

the hotspot temperature constraint must be considered for reactor thermal stability. In Fig. 6 reactor temperature profiles for different shell temperatures are plotted.

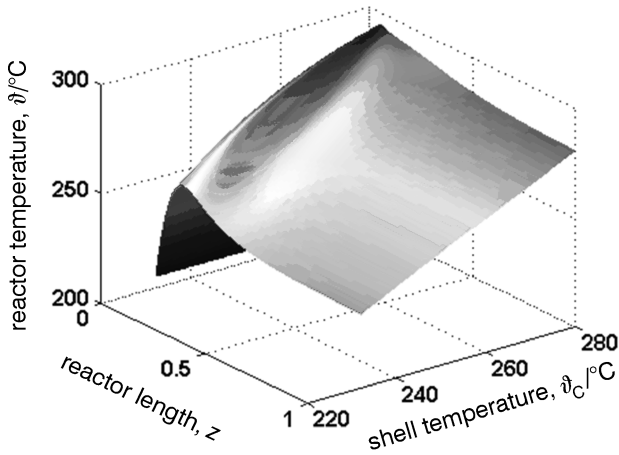


Fig. 6 – Effect of shell temperature on reactor temperature profile along the reactor length

Steady-state optimizer

To find the optimum shell temperature for DME production an objective function which is DME productivity is considered. For a given feed condition, the optimizer calculates the optimum shell temperature, which maximizes the DME productivity by considering the maximum allowable temperature to avoid catalyst deterioration. By changing the feed properties, the optimizer recalculates the new optimum shell temperature. The optimization problem is defined below:

$$\text{maximize}_{T_C} \text{PI} = F_{\text{DME}} \frac{MW_{\text{DME}}}{m_{\text{catalyst}}}$$

subject to

$$T_{\text{reactor, max}} < 543 \text{ K}$$

$$505 \text{ K} \leq T_C$$

where F_{DME} is DME outlet mole flow rate, MW_{DME} is DME molecular mass and m_{catalyst} is mass of catalyst in the reactor. The above objective function is DME productivity and T_C is the decision variable. The first constraint is considered to avoid hotspot in the reactor and the second constraint is due to required quality of the produced vapor.¹⁸ For optimization purposes the genetic algorithm (GA) given in the Genetic Algorithm and Direct Search Toolbox of MATLAB with its default options and parameters has been used. The genetic algorithm can be used for solving both constrained and uncon-

strained optimization problems. This technique is based on natural selection, the process that drives biological evolution. The genetic algorithm repeatedly modifies a population of individual solutions. At each step, the individuals are selected randomly from the current population to be parents and used to produce the children for the next generation. Over successive generations, the population “evolves” towards an optimal solution.

By solving the above optimization problem, the shell temperature that maximizes DME productivity is obtained. Having the optimum shell temperature, the corresponding optimum shell pressure is calculated and used as a pressure set-point for the pressure control loop. By controlling the steam drum pressure at the optimum calculated pressure, the DME productivity is maximized for a given feed condition. When feed composition changes, the optimizer becomes active and calculates the new optimum steam drum pressure. The schematic diagram of the optimizer coupled with the process is shown in Fig. 7.

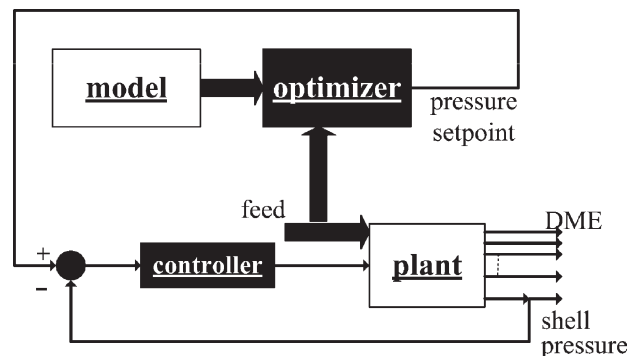


Fig. 7 – Schematic diagram of optimizer coupled with the process

Reactor open loop response

To investigate the effect of manipulated variable (steam flow rate) on the reactor performance, step changes in different directions are applied to steam flow rate. Variations of shell pressure, maximum reactor temperature and DME production rate are shown in Fig. 8. As can be seen from Fig. 8a, shell pressure dynamic is almost linear, and therefore a traditional PID controller can be used for pressure loop, which is discussed in the next part. Fig. 8b shows that, the reactor maximum temperature is increased as the shell pressure increases which is reasonable. As can be seen from Fig. 8c, changing the shell pressure has a direct effect on DME production rate. This can be explained as follows. The shell temperature corresponding to initial shell pressure is 247 °C. As can be seen from Fig. 5 this temperature lies on the left hand side of the op-

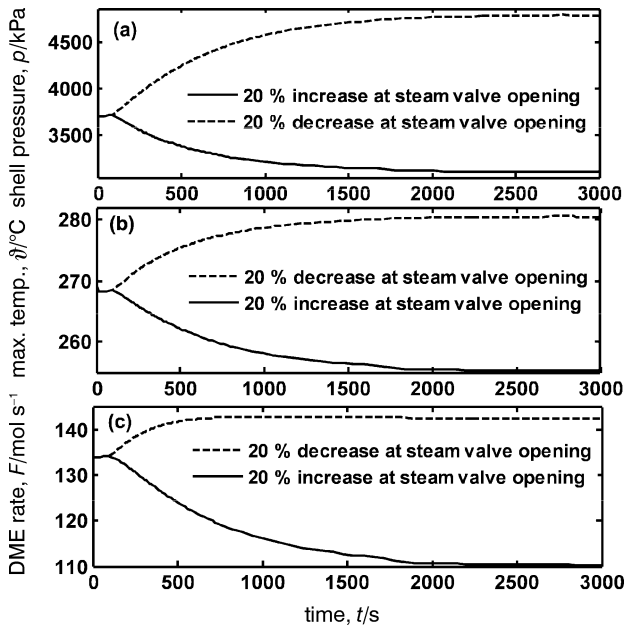


Fig. 8 – Open loop responses for step changes in the steam flow rate a) shell pressure, b) reactor maximum temperature, c) DME production rate

imum shell temperature where increasing the shell temperature results an increase in DME production rate.

Reactor control strategy

The main control objective is controlling the reactor temperature. Cooling water flows through the reactor shell and absorbs heat of reaction and produces steam. For controlling the shell temperature, the pressure (having a faster dynamic) is being controlled because for saturated steam, pressure and temperature are related. To keep the level constant in the steam drum, a level control loop was considered. These loops are shown in Fig. 1. Both controllers are PI controller.

For controlling the steam drum level, the water make up flow rate is manipulated and the steam drum pressure is controlled by manipulating the steam outlet flow rate. The PI controllers are tuned using quarter decay method. The PI parameters are given in Table 4. To improve the performance of the pressure controller, a PI controller with an anti-windup scheme was used. Fig. 9a shows the pressure closed loop response for the set point

Table 4 – PI controller parameters

Controller	τ_i/s	K_c
pressure loop	0.58485	336.45
level loop	9	-8.5

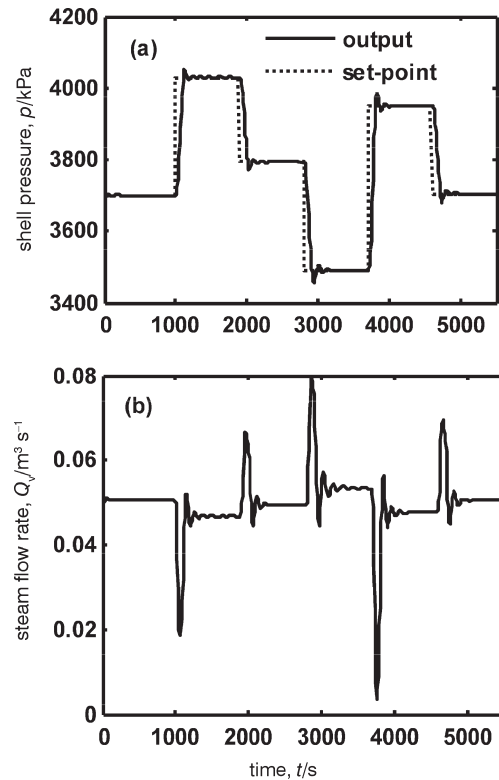


Fig. 9 – Closed loop response for set-point tracking a) shell pressure vs. time, b) steam flow rate vs. time

tracking, and Fig. 9b shows its corresponding control action.

Production rate optimization

Closed loop responses are investigated for two cases. In the first case, the optimizer is active when feed composition is changed, while in the second case, the optimizer is off and changes in feed composition are considered as disturbances and the pressure loop set-point is fixed.

The nominal feed composition (A) and two other feed compositions (B and C) are given in Table 5. It is assumed that feed composition changes from A to B at $t = 1000$ s and then from B to C at $t = 3000$ s.

Table 5 – Different feed compositions

Component	Mole fraction, $x_i/\%$		
	A	B	C
H ₂	68.47	71.24	64.94
CO	23.10	19.37	26.49
CO ₂	6.96	7.30	6.65
H ₂ O	0.18	0.57	0.52
N ₂	0.29	0.48	0.44
CH ₄	0.98	1.03	0.94

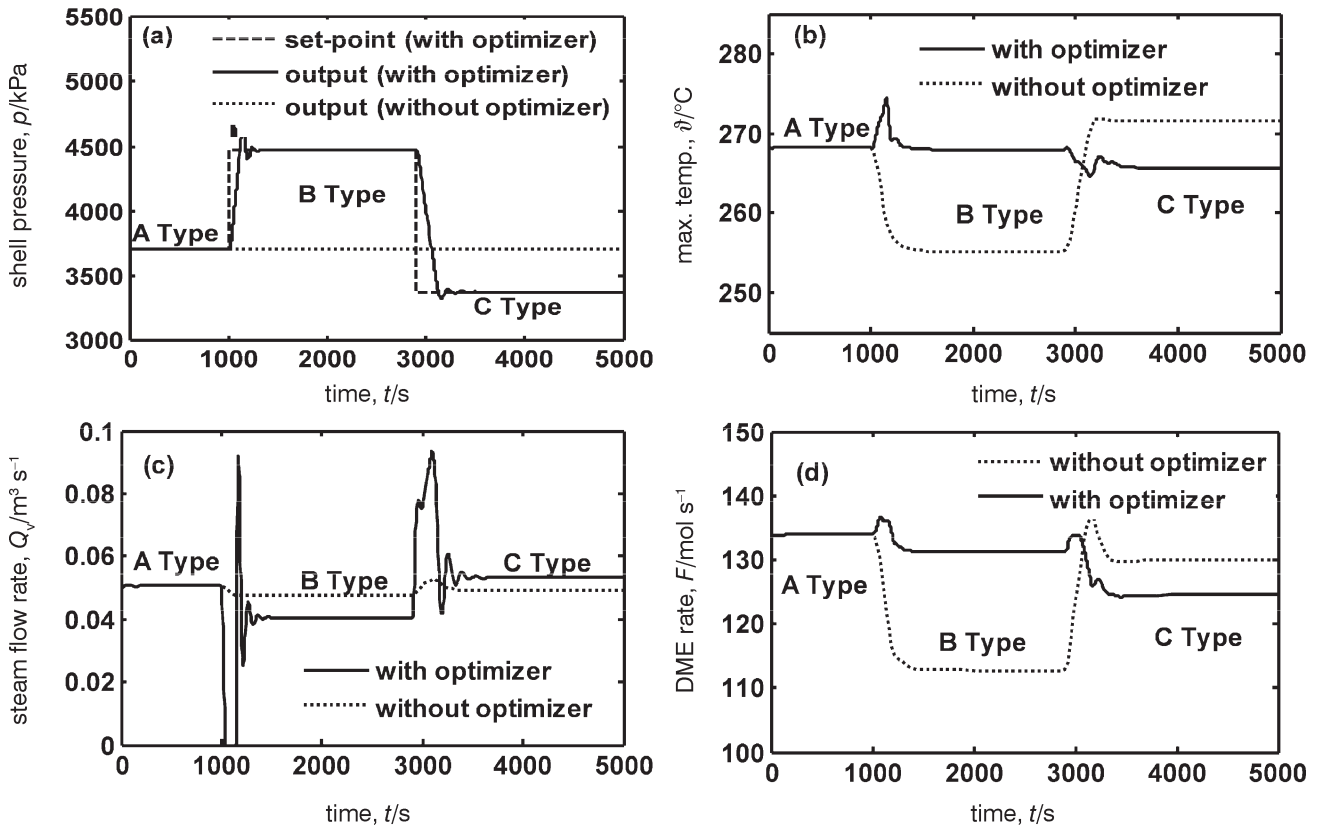


Fig. 10 – Comparison of closed loop responses with and without optimizer a) optimal pressure set-point and pressure loop responses, b) maximum reactor temperature, c) steam flow rate, d) DME production rate

The optimal set point trajectory and pressure closed-loop response are shown in Fig. 10a. The corresponding maximum reactor temperatures and steam flow rate for two cases are shown in Figs. 10b and 10c. As can be seen, the optimizer prevents the temperature from exceeding the limit (Fig. 10b) and also maximizes DME production (Fig. 10d). For DME synthesis, the temperature should not exceed 270°C .³ As can be seen from Fig. 10d, for C type feed without using the optimizer, DME production is higher but the maximum reactor temperature is exceeded. This fact justifies application of the proposed optimizer.

Conclusion

In this study, production of DME in a catalytic fixed-bed shell and tube reactor has been considered. Mass and energy conservation laws plus kinetic equations were used for reactor modeling. Due to the highly exothermic nature of reactions involved in production of DME, a catalytic shell and tube fixed-bed reactor similar to the Lurgi methanol reactor was used. This kind of reactor can provide efficient temperature control and heat removal from the reactor. For controlling the reactor, two control loops (level and pressure) were considered. To

maximize the DME production rate, an optimizer that takes into account the feed variations was proposed. Simulation results indicate that the control system including the optimizer keeps the production rate at the maximum value without exceeding the temperature limit.

Nomenclature

- A_T – tube cross-section area, m^2
- c_i – concentration of the i^{th} component, mol m^{-3}
- $c_{p,g}$ – specific heat capacity of gas, $\text{J kg}^{-1} \text{K}^{-1}$
- $c_{p,l}$ – specific heat capacity of liquid, $\text{J kg}^{-1} \text{K}^{-1}$
- $c_{p,s}$ – specific heat capacity of solid, $\text{J kg}^{-1} \text{K}^{-1}$
- $\hat{C}_{p,m}$ – mean specific heat of bed, $\text{J m}^{-3} \text{K}^{-1}$
- d_p – equivalent diameter of catalyst particle, m
- d_{out} – external diameter of tube, m
- f_i – fugacity of i^{th} component, bar
- F – mole flow rate, mol s^{-1}
- h_m – enthalpy of makeup water, J kg^{-1}
- h_s – enthalpy of steam, J kg^{-1}
- K_i – adsorption constant, bar^{-1}
- K_{fi} – equilibrium constant, reaction dependent
- k_i – reaction rate constant, reaction dependent
- K_{MT} – pseudo mass transfer coefficient, m s^{-1}
- K_V – control valve constant, $\text{m}^4 \text{s kg}^{-1}$

L_r – reactor length, m
 m – mass of catalyst, kg
 MW_{water} – molecular mass of water, kg kmol⁻¹
 n_{0i} – inlet mole flow rate of i^{th} component, mol s⁻¹
 n_i – reactor mole flow rate of i^{th} component, mol s⁻¹
 P – productivity, g g⁻¹ h⁻¹
 p_0 – inlet pressure of control valve, bar
 p_i – partial pressure of i^{th} component, bar
 q_w – water boiling rate, kg s⁻¹
 Q_m – volume flow rate of makeup, m³ s⁻¹
 Q_V – volume flow rate of vapor, m³ s⁻¹
 R – gas constant, J mol⁻¹ K⁻¹
 r_i – reaction rate, mol s⁻¹ kg⁻¹
 t – time, s
 T – temperature, K
 u_s – gas velocity, m s⁻¹
 U_{eff} – overall heat transfer coefficient, W m⁻² K⁻¹
 V_l – liquid phase volume, m³
 V_v – vapor phase volume, m³
 X – conversion, %
 x_i – mole fraction of i^{th} component
 z – reactor dimensionless length
 ΔH_i – heat of i^{th} reaction, J mol⁻¹
 Φ_R – heat removed from the reactor, J s⁻¹
 ϑ – reactor temperature, °C
 ϑ_c – shell temperature, °C
 ε – bed porosity
 μ_g – gas phase viscosity, kg m⁻¹ s⁻¹
 ν – stoichiometric number
 ρ_b – bed density, kg m⁻³
 ρ_g – gas density, kg m⁻³
 ρ_l – liquid density, kg m⁻³
 ρ_m – density of makeup, kg m⁻³
 ρ_v – vapor density, kg m⁻³

ρ_s – solid density, kg m⁻³

References

- Galvita, V. V., Semin, G. L., Belyaev, V. D., Yurieva, T. M., Sobyenin, V. A., *Appl. Catal. A* **216** (2001) 85.
- Tartamella, T. L., Lee, S., *Technol.* **38** (4) (1997) 228.
- Lu, W.-Z., Teng, L.-H., Xiao, W.-D., *Chem. Eng. Sci.* **59** (2004) 455.
- Brown, D. M., Bhatt, B. L., Hsiung, T. H., *Catal. Tod.* **8** (1991) 279.
- Du, M. X., Li, Y. W., Hu, H. M., *Coal Conversion* **16** (4) (1993) 68.
- Guo, J. W., Niu, Y. Q., Zhang, B. J., *Natural Gas Chem. Ind.* **25** (2000) 4.
- Lee, E. S., *Chem. Eng. Sci.* **21** (1996) 143.
- Cresswell, D. L., Paterson, W. R., *Chem. Eng. Sci.* **25** (1970) 1405.
- Balakotaiah, V., Christoforatos, E. L., West, D. H., *Chem. Eng. Sci.* **54** (1999) 1725.
- Shahrokhi, M., Baghmisheh, G. R., *Chem. Eng. Sci.* **60** (2003) 4275.
- Lee, S. B., Cho, W., Park, D. K., Yoon, E. S., *Korean Journal of Chem. Eng.* **23** (4) (2006) 522.
- Song, D., Cho, W., Lee, G., Park, D. K., Yoon, E. S., *Ind. and Chem. Eng. Res.* **47** (2008) 4553.
- Nie, Z., Liu, H., Liu, D., Ying, W., Fang, D., *Journal of Natural Gas* **14** (2005) 22.
- Jia, G., Tan, Y., Han, Y., *Ind. Eng. Chem. Res.* **45** (2006) 1152.
- Erena, J., Garona, R., Arandes, J. M., Aguayo, A. T., Bilbayo, J., *Catal. Tod.* **107** (2005) 467.
- Luyben, W. L., *Process Modeling, Simulation and Control for Chemical Engineering*, McGraw-Hill, 1986.
- Fred Ramirez, W., *Computational Methods for Process Simulation*, 2nd Edition, McGraw-Hill, 1997.
- Lovik, I., *Modeling, estimation and optimization of the methanol synthesis with catalyst deactivation*. Ph.D. Thesis, Norwegian University of Science and Technology, 2001.

